

# Effect of fault damage zones on long-term earthquake behavior on mature strike-slip faults

P. Thakur<sup>1</sup>, Y. Huang<sup>1</sup>, Y. Kaneko<sup>2</sup>

<sup>1</sup>University of Michigan, Department of Earth and Environmental Sciences  
<sup>2</sup>GNS Science, New Zealand

## Key Points:

- Fully dynamic earthquake cycle simulations show persistent heterogeneous stress distribution generated by low-velocity fault zone waves
- Faults surrounded by low-velocity damage zones lead to more complex patterns of earthquakes
- Shallower damage zones tend to have shallower earthquake hypocenters

This paper is a non-peer reviewed preprint submitted to *JGR:Solid Earth*.

**Abstract**

Mature strike-slip faults are usually surrounded by a narrow zone of damaged rocks characterized by low seismic wave velocities. Observations of earthquakes along such faults indicate that seismicity is highly concentrated within this fault damage zone. However, the long-term influence of the fault damage zone on complete earthquake cycles, i.e., years to centuries, is not well understood. We simulate aseismic slip and dynamic earthquake rupture on a vertical strike-slip fault surrounded by a fault damage zone for a thousand-year timescale using observations along major strike-slip faults, e.g., San Andreas Fault, as constraints on fault zone material properties and geometry. We find that dynamic wave reflections, whose characteristics are strongly dependent on the width and the rigidity contrast of the fault damage zone, have a prominent effect on the stressing history of the fault. The presence of elastic damage can explain, in part, the variability in the earthquake sizes and hypocenter locations along a single fault, which vary with fault damage zone depth, width and rigidity contrast from the host rock. The depth extent of the fault damage zone has a pronounced effect on the earthquake hypocenter locations, and shallower fault damage zones favor shallower hypocenters with a possible bimodal distribution of seismicity along depth. Our findings also suggest significant fault damage zone effects on the hypocenter distribution when the fault damage zone penetrates to the nucleation sites of earthquakes. Therefore the depth distribution of seismicity in mature strike-slip faults is likely influenced by both lithological (material) and rheological (frictional) boundaries.

**Plain Language Summary**

Large strike-slip earthquakes tend to create a zone of fractured network surrounding the main fault. This zone, referred to as a fault damage zone, becomes highly localized as the fault matures, spanning several hundred meters in width. The influence of this fault damage zone on earthquake characteristics remains elusive since we do not have enough long-term observations along a single fault. We use numerical simulations to examine the behavior of earthquake nucleation and rupture dynamics on a fault surrounded by a damage zone over a thousand-year timescale. Our simulations reveal that the reflection of seismic waves from the fault damage zone boundaries leads to complexity in earthquake sequences, such as variability in earthquake locations and sizes. We also show that a shallow fault damage zone produces shallower earthquakes with the earthquake depths centered around two locations (bimodal), as opposed to a deep fault damage zone with the earthquake depths centered around a single location (unimodal). Our study suggests that imaging the geometry and physical properties of fault damage zones could potentially give us clues about depths of future earthquakes and improve earthquake probabilistic hazard assessment.

**1 Introduction**

Natural faults are often approximated as a single plane of intense deformation, macroscopically seen as a principal slip surface. However, geological (e.g., F. Chester and Logan (1986); F. M. Chester et al. (1993); Lockner et al. (2011)), geophysical (e.g., Li and Leary (1990); Unsworth et al. (1997); Lewis and Ben-Zion (2010)), and geodetic (e.g., Fialko et al. (2002)) observations delineate faults as a geometrically complex network of multiple slip surfaces and fractures, with a nested hierarchy of increasing deformation towards the principal slip surface (Fig. 1). These damaged rocks exhibit a dense network of fractures which can be macroscopically approximated as an elastic zone with reduced shear modulus and seismic velocities (F. M. Chester et al., 1993; Harris & Day, 1997). The damage zones, exhibiting sharp contrast of seismic velocities with respect to the host rock, are capable of trapping seismic waves. The fault damage zone can potentially promote complex stress distribution along faults due to its pronounced dynamic effect on earthquake rupture nucleation and propagation (e.g., Harris and Day (1997); Huang and Ampuero (2011); Huang et al. (2014); Ma and Elbanna (2015); Albertini and Kammer (2017); Weng et al. (2016); Huang (2018)).

63 We aim to understand the dynamic effects of the fault damage zone over earthquake cycles,  
 64 which include interseismic slip, earthquake nucleation, rupture propagation, and postseismic  
 65 slip, and study its influence on the variability in earthquake sizes, recurrence intervals and  
 stressing history of the fault.

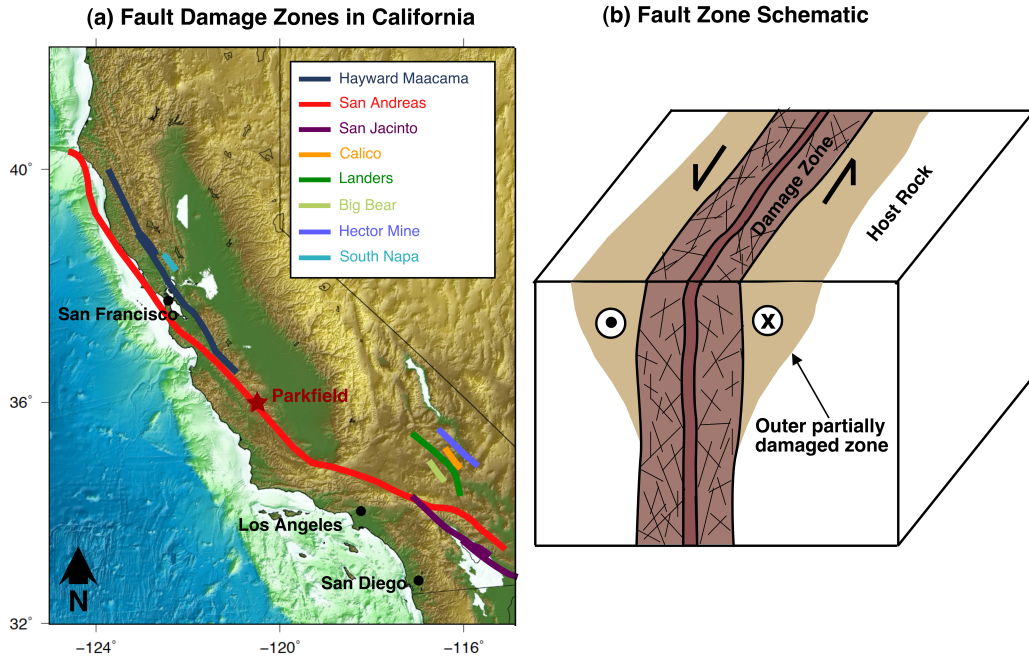


**Figure 1.** (a) Map of California faults with documented fault damage zones. (b) A schematic of mature fault zone structure that includes a fault core shown as the central red zone surrounded by an inner narrow zone of damage extending through the seismogenic zone, and an outer partially-damaged zone resembling a flower structure. Our models represent a two-dimensional vertical cross section across the fault.

66

67 Previous numerical models in homogeneous medium (Rundle & Jackson, 1977; Rundle,  
 68 1989) and experiments (Mogi, 1962; C. Scholz, 1968) showed that both mechanical proper-  
 69 ties of fault rocks and fault stresses can greatly contribute to the variability in earthquake  
 70 magnitudes and the power-law behavior of the magnitude-frequency distribution. Dynamic  
 71 models of multiple spring-block sliders (Carlson & Langer, 1989; Shaw, 1995) have been  
 72 successful in reproducing the Gutenberg-Richter distribution and non-uniform recurrence  
 73 times. These models do not assume any structural or material heterogeneities, thus imply-  
 74 ing that such complexities are a sole manifestation of fault friction. Quasi-dynamic  
 75 continuum models in homogeneous medium, however, have been unable to reproduce such  
 76 complexities from fault friction alone, unless extreme values of frictional parameters are  
 77 considered (Cochard & Madariaga, 1996; Hillers et al., 2006). Erickson and Dunham (2014)  
 78 incorporated a heterogeneous medium in quasi-dynamic earthquake cycle simulations in the  
 79 form of a sedimentary basin and showed the emergence of sub-surface events in addition to  
 80 surface breaking events. Abdelmeguid et al. (2019) have shown the generation of subsur-  
 81 face events and multi-period sequences in a low-velocity layered fault damage zone. More  
 82 recently, Idini and Ampuero (2020) (EarthArXiv preprint) showed complex rupture patterns  
 83 and back-propagating secondary rupture fronts due to fault zone damage persistent during  
 84 multiple earthquake cycles in a quasi-dynamic approximation of earthquake sequences. Here

85 we consider fully dynamic continuum models with fault damage zone surrounding mature  
 86 strike-slip faults. Using fully dynamic earthquake cycle simulations, Kaneko et al. (2011)  
 87 showed that a fault-parallel, narrow damage zone causes a reduction in the nucleation size  
 88 of the earthquakes and amplification of slip rates during dynamic earthquake events. De-  
 89 spite multitude of studies documenting the effects of fault damage zones on single rupture  
 90 (Harris & Day, 1997; Huang & Ampuero, 2011; Huang et al., 2014), their long-term effects  
 91 on earthquake sequences are not well understood, partially owing to a lack of seismological  
 92 records over centuries.

93 We model earthquake sequences with full inertial effects on a two-dimensional vertical  
 94 strike-slip fault surrounded by a fault damage zone. The constitutive response of the fault is  
 95 governed by laboratory derived rate-and-state friction laws (Dieterich, 1979; Ruina, 1983).  
 96 This fully dynamic modeling approach can simulate interseismic slip, earthquake nucleation,  
 97 rupture propagation and postseismic deformation during multiple seismic cycles in a single  
 98 computational framework (e.g., Lapusta et al. (2000); Kaneko et al. (2011); Barbot et al.  
 99 (2012); Jiang and Lapusta (2016)). We investigate how the wave reflections from fault dam-  
 100 age zone influences the long-term stress evolution and explain the variability in earthquake  
 101 magnitudes and hypocenter locations. We show that the variability in earthquake hypocen-  
 102 ter is significant only in the cases where the damage zone truncates close to the nucleation  
 103 site or extends beyond the nucleation zone, suggesting that frictional and rheological effects  
 104 may be a dominant mechanism for hypocenter variability when the damaged structure is  
 105 very shallow. Our results also provide a possible explanation for the bimodal depth dis-  
 106 tribution of seismicity observed along mature strike-slip faults with shallow fault damage  
 107 zone structures. We describe the observed geometry and material properties of the fault  
 108 damage zone along the San Andreas Fault that inspire the design of our simulations in sec-  
 109 tion 2. The two-dimensional model setup, model assumptions, friction laws, and simulation  
 110 methodology are presented in section 3. We demonstrate the effects of the fault damage  
 111 zone with varying widths and rigidity contrasts on the variability of earthquake magnitudes  
 112 and hypocenters in section 4.

## 113 2 Observed dimension and material properties of fault damage zones

114 Fault damage zones can be delineated using potential field methods and seismic observa-  
 115 tions based on trapped waves within the damaged zone. Seismic reflections, magnetotelluric  
 116 and resistivity surveys along the Parkfield segment of San Andreas Fault reveal a 500 m  
 117 wide and 4 km deep fault damage zone (Unsworth et al., 1997). This study also suggests  
 118 a presence of a deeper fault zone whose property is not well resolved, and a shallow 5 km  
 119 wider damage zone surrounding the  $\sim$ 500 m wide damage zone, representing a flower struc-  
 120 ture. Other studies along San Jacinto Fault Zone and San Andreas Fault Zone (e.g., Li and  
 121 Vernon (2001); Wu et al. (2010)) also indicate that the low-velocity zone may extend to  
 122 seismogenic depths. Fault zone trapped wave studies along the Parkfield segment (Lewis &  
 123 Ben-Zion, 2010) indicate a 3 km to 5 km deep, 150 m to 300 m wide fault damage zone, with  
 124 a potentially nested fault zone extending up to 7 km to 10 km. Geologic interpretations on  
 125 the same region from the SAFOD cores (Lockner et al., 2011) delineate a  $\sim$ 200 m wide fault  
 126 damage zone at 2.7 km depth. A detailed 3-D seismic wave velocity map (Thurber et al.,  
 127 2003) also reveals a several hundred meters wide fault zone structure at about 5 km to 8 km  
 128 depth. The shear wave velocity contrast between the host rock and the fault damage zone  
 129 is found to be around 10% to 60% (table 1 in Huang et al. (2014) and references therein).  
 130 Most of these studies report variations in fault damage zone structure along fault strike.  
 131 We summarize the observed fault damage zone geometry along the Parkfield segment in  
 132 Table 1. Based on this review, it is clear that the fault damage zone width spans several  
 133 hundred meters, whereas the depth extent is more debatable since the narrow damage zone  
 134 is more difficult to resolve at depth. We use these observations to guide our model setup as  
 135 described in the following section.

**Table 1.** Geometry of fault damage zone along Parkfield segment of San Andreas Fault as constrained by different studies.

References	Geometry	Width Inference	Depth Inference
Resistivity and MT (Unsworth et al., 1997)	Wide at the top, narrow at depth	500 m for inner damage, 5 km for outer damage	4 km, with a deeper damage zone less resolved
Trapped seismic waves (Lewis & Ben-Zion, 2010)	Tabular low velocity zone	150 m to 300 m	5 km to 7 km
Seismic wave velocities (Thurber et al., 2003)	Wide at the top and at seismogenic depth, narrow in between	500 m to 600 m	8 km
Geology: SAFOD (Lockner et al., 2011)	Tabular	200 m	2 km

### 3 Methodology

#### 3.1 Model Description

We consider a two-dimensional strike-slip fault embedded in an elastic medium with mode III rupture Fig. 2. This implies that the fault motion is in and out of the plane and only the depth variations of parameters are considered. The top boundary is stress-free and represents earth's free surface. The other three boundaries are absorbing boundaries that allow the waves to pass through. Since our model is symmetric across fault, we restrict the computational domain to only one side of the fault. Our domain extends to 48 km depth, where the top 24 km of the fault is bordered at the bottom by a region constantly slipping at  $35 \text{ mm yr}^{-1}$ . This represents the tectonic plate motion that loads the fault and accumulates stresses. The seismogenic zone extends from 2 km to 15 km, which is locked during the interseismic period and capable of hosting earthquakes. The rest of the fault creeps aseismically. Earthquakes are captured in our simulations when the maximum slip velocity on the fault exceeds the threshold of  $0.001 \text{ mm s}^{-1}$ . This model is inspired by the San Andreas fault, and is similar in setup to Lapusta et al. (2000) and Kaneko et al. (2011).

The fault damage zone is modeled as an elastic layer with lower seismic wave velocities compared to the host rock. We will focus on how the geometry, spatial extent, and damage intensity of this fault damage zone influence the earthquake sequence behavior. We consider four different scenarios: (I) a homogeneous elastic medium as a reference model, (II, III) a medium with a sharp, narrow fault damage zone with various depths, widths and velocity contrasts that extends throughout the seismogenic depth in model II and truncates at a shallow depth in model III, and (IV) a flower structure in which a narrow fault damage zone extending through the domain surrounded by a wider, trapezium-shaped fault damage zone truncated at a shallow depth (Fig. 2). In natural settings, the outer trapezium-shaped fault damage zone may not have a sharp boundary at depth but may show a smooth transition because its structure is more diffused than the inner fault damage zone. We use a sharp boundary as an approximation of the flower structure in order to highlight the effects of dynamic wave reflections. These four sets of models are described in Fig. 2. We vary the width ( $H$ ) and shear wave velocity ( $c_s$ ) contrast of the fault damage zone in the Model (II) and the depth ( $D$ ) in model III to study their effects on earthquake sizes and hypocenters (Fig. 2a). The choices of ' $H$ ' and ' $c_s$ ' are shown in Fig. 3. We choose four different values of ' $D$ ' including two depths (6 km and 8 km) shallower than the nucleation

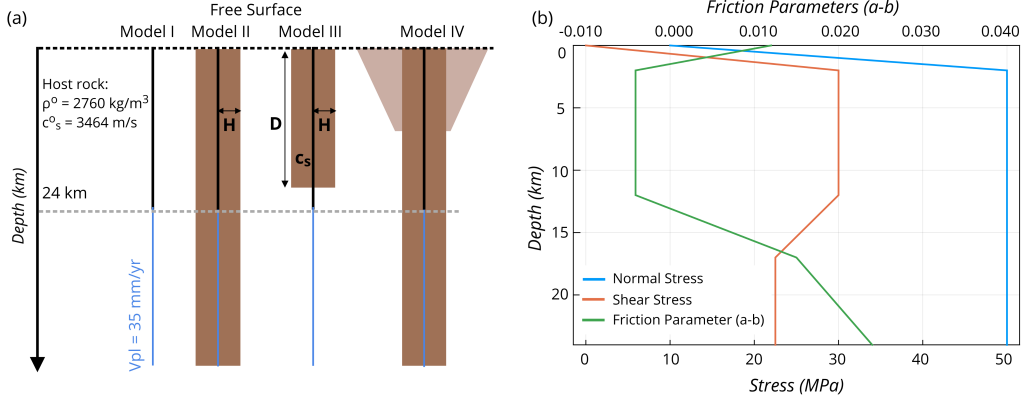


**Figure 2.** (a) Model description of four different scenarios. We consider a vertical strike-slip fault 24 km deep loaded from below by a plate motion rate of  $35 \text{ mm yr}^{-1}$ . Model I: Homogeneous medium used as a reference model. Model II: A narrow fault damage zone extending throughout the seismogenic zone. Model III: A narrow fault damage zone truncating at a shallower depth, and Model IV: Two-dimensional approximation of flower structure damage. (b) Friction parameters ( $a - b$ ) and initial stresses along the fault dip. The seismogenic zone, i.e., the velocity weakening region, is the overstressed patch between 2 and 15 km depth.

168 site in the homogeneous medium, one depth intersecting the nucleation zone (10 km) and  
 169 one depth extending beyond the nucleation zone (12 km). In the Model (IV), the outer,  
 170 wider fault damage zone has a shear wave velocity reduction of 20 % compared to the host  
 171 rock, while the inner one has a 40 % reduction. The second and third models are inspired  
 172 by the geological and geophysical observations of the San Andreas fault zone as discussed  
 173 in section 2, and the fourth model is inspired by the classic flower structure of fault damage  
 174 zones (Sibson, 1977; Unsworth et al., 1997; Caine et al., 1996; Pelties et al., 2015; Perrin et  
 175 al., 2016).

### 3.2 Friction Laws

176 We use laboratory-derived rate and state friction laws to describe the fault slip (Dieterich,  
 177 1979; Ruina, 1983; C. H. Scholz, 1998). This friction law relates the shear strength ( $T$ ) on  
 178 the fault to the slip rate ( $\dot{\delta}$ ) as follows:  
 179

$$180 \quad T = \bar{\sigma} \left[ f_o + a \ln \left( \frac{\dot{\delta}}{\dot{\delta}_o} \right) + b \ln \left( \frac{\dot{\delta}_o \theta}{L} \right) \right] \quad (1)$$

181 where  $\bar{\sigma}$  is the effective normal stress (the difference between lithostatic stress and the pore  
 182 fluid pressure),  $f_o$  is a reference friction coefficient corresponding to a reference slip rate  $\dot{\delta}_o$ ,  
 183 and  $a$  &  $b$  are empirical constants dependent on the mechanical and thermal properties of  
 184 the contact surface. The parameter  $\theta$  is a state variable interpreted as the average lifetime  
 185 of the surface in contact, and  $L$  is the characteristic distance over which the contact surface  
 186 slips. The term  $a \ln \left( \frac{\dot{\delta}}{\dot{\delta}_o} \right)$  is called the direct effect term, and the term  $b \ln \left( \frac{\dot{\delta}_o \theta}{L} \right)$  is the  
 187 state evolution term (Eq. 1). The state variable  $\theta$  is intuitively hard to understand, so the  
 188 term  $f_o + b \ln \left( \frac{\dot{\delta} \theta}{L} \right)$ , referred to as  $\psi$  is commonly used to interpret the state evolution  
 189 term and is defined as the current absolute offset of the friction coefficient. The frictional  
 190 stability of faults is determined by two frictional parameters,  $L$  and  $(a - b)$ . Depending  
 191 on the value of  $(a - b)$ , we can have an unstable slip for a steady state velocity weakening  
 192 frictional regime  $(a - b) < 0$ , or a stable sliding for a steady state velocity strengthening

193 frictional regime ( $a - b > 0$ ). Earthquakes occur when the velocity-weakening region of the  
 194 fault exceeds a critical nucleation size that depends on the shear moduli of near-fault rocks,  
 195 effective normal stress and frictional parameters (Rice, 1993; Rubín & Ampuero, 2005). The  
 196 evolution of the state variable is governed by the aging law:

$$197 \quad \frac{d\theta}{dt} = 1 - \frac{\dot{\delta}\theta}{L} \quad (2)$$

198 Since the above formulation (Eq. 1) has singularity at slip rate  $\dot{\delta} = 0$ , we use a regularized  
 199 formulation for the shear strength, which is interpreted as a thermally activated creep model  
 200 for the term  $a \ln(\frac{\dot{\delta}}{\dot{\delta}_o})$  in Eq. 1 (Rice & Ben-Zion, 1996; Lapusta et al., 2000):

$$201 \quad T = a\bar{\sigma} \operatorname{arcsinh} \left[ \frac{\dot{\delta}}{2\dot{\delta}_o} e^{\frac{f_o + b \ln(\dot{\delta}\theta/L)}{a}} \right] \quad (3)$$

202 We use a depth dependent profile for  $(a - b)$  as inferred from granite samples in laboratory  
 203 experiments (M. Blanpied et al., 1991; M. L. Blanpied et al., 1995). The seismogenic zone  
 204 is the velocity weakening region extending from a depth of 2 km to 15 km. The rest of the  
 205 fault is velocity strengthening and accommodates aseismic creep. The velocity strengthening  
 206 region at the top 2 km of the fault is suggested by laboratory observations under low stresses  
 207 (M. Blanpied et al., 1991). The effective normal stress is constant below the depth of 2 km,  
 208 since the increase in the lithostatic stress is accommodated by the pore fluid pressure at  
 209 depth (Rice, 1993). The seismogenic zone is overstressed initially (Fig. 2b).

### 210 **3.3 Numerical Simulation of Fully Dynamic Earthquake Sequences**

211 We use a spectral element method to simulate dynamic ruptures and aseismic creep on  
 212 the fault (Kaneko et al., 2011). Full inertial effects are considered during earthquake rupture  
 213 and an adaptive time stepping technique is used to switch from interseismic to seismic events  
 214 based on a threshold maximum slip velocity on the fault. This method is able to capture all  
 215 four phases of the earthquake cycle including nucleation, rupture propagation, post seismic  
 216 deformation, and interseismic creep. We implement Kaneko et al. (2011)'s algorithm in Julia  
 217 (Bezanson et al., 2017) using a more efficient linear solver based on the Algebraic Multigrid  
 218 scheme (Ruge & Stüben, 1987) for the elliptic (interseismic) part of the earthquake sequence.  
 219 This iterative technique uses a fixed number of iterations independent of the mesh size. In  
 220 addition, we use the built-in multithreading feature of Julia, which enables us to achieve  
 221 a CPU speed-up of  $\sim 50$  times compared to the original code described in Kaneko et al.  
 222 (2011).

### 223 **3.4 Theoretical Nucleation Estimates and choice of $L$**

224 In a two-dimensional continuum model, the theoretical estimate of earthquake nucle-  
 225 ation for a mode III crack based on energy balance is given by (Rubín & Ampuero, 2005):

$$226 \quad h^* = \frac{2}{\pi} \frac{\mu L b}{\bar{\sigma}(b - a)^2} \quad (4)$$

227 where  $a, b$ , and  $L$  are the rate and state friction parameters,  $\mu$  is the shear modulus of  
 228 the near source region and  $\bar{\sigma}$  is the effective normal stress. Using  $L = 8$  mm leads to a  
 229 nucleation size of 3.9 km in a homogeneous medium. As the nucleation size is proportional  
 230 to the rigidity of the near-source medium (Rubín & Ampuero, 2005; Kaneko et al., 2011),  
 231 it is reduced by a factor of  $\sim 3$  in a damaged medium with a shear wave velocity reduction  
 232 of 40% (Huang, 2018). The theoretical estimate of the nucleation size in a layered medium  
 233 for a mode III rupture is derived by Kaneko et al. (2011) using linear stability analysis:

$$234 \quad h_{lay}^* \tanh \left[ 2H \frac{\gamma}{h_{lay}^*} + \operatorname{arctanh} \left( \frac{\mu_D}{\mu} \right) \right] = h_{hom}^* \quad (5)$$

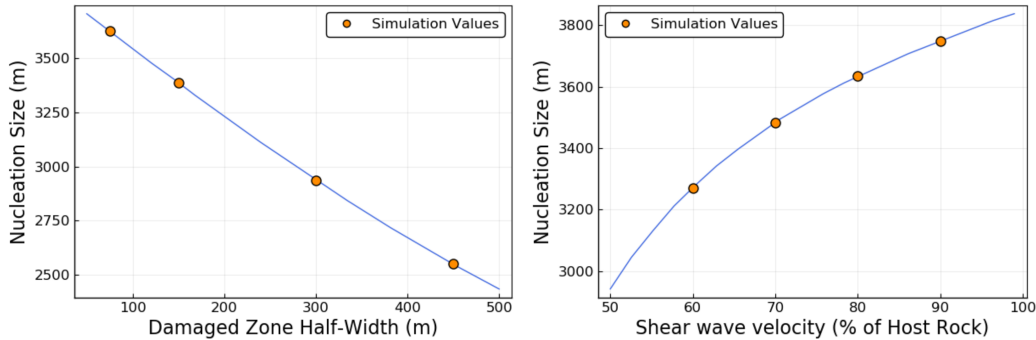


**Figure 3.** Variation of theoretical nucleation sizes in a layered medium. The left figure shows the variation due to fault damage zone widths, and the right figure shows the variation due to shear wave velocity. The orange dots show the theoretical nucleation sizes for the parameters chosen in our simulations.

235 where  $\mu$  and  $\mu_D$  are the rigidity of the host rock and the layer respectively,  $\gamma$  ( $= \pi/4$ ) is  
 236 an empirical parameter dependent on the geometry, and  $H$  is the thickness of the layered  
 237 medium. The parameter choice of width and shear wave velocity contrast and their corre-  
 238 sponding nucleation sizes are shown in Fig. 3. A smaller nucleation size would allow smaller  
 239 earthquakes to nucleate successfully, therefore incorporating a wider range of magnitudes.  
 240 We use 5 Gauss-Lobatto-Legendre nodes inside each spectral element, such that the average  
 241 node spacing is 20 m. For a well resolved simulation, the cohesive zone size (Day et al., 2005;  
 242 Kaneko et al., 2008) should contain at least 3 node points. Based on the frictional param-  
 243 eters and rigidity of fault damage zone, the cohesive zone size in our models is  $\sim 120$  m and  
 244 encompasses sufficient nodes. We demonstrate the convergence of our model with respect to  
 245 different node spacings in Appendix A.

## 246 4 Results

247 Our results show that the presence of the fault damage zone promotes complexity in the  
 248 earthquake slip distribution and variability in their magnitudes, especially for large rigidity  
 249 contrast between the fault damage zone and the host rock. Given the friction parameters  
 250 and initial stress conditions in our simulations (Fig. 2b), the homogeneous medium hosts  
 251 periodic earthquakes with exactly the same hypocenter locations and magnitudes, whereas  
 252 the fault surrounded by a fault damage zone shows a more complex slip distribution with  
 253 variable earthquake sizes and hypocenter locations through multiple earthquake cycles (Fig.  
 254 4). We also observe ruptures with multiple slip pulses and more complex slip distribution  
 255 in the flower structure scenario (Fig. 4d, Fig. 5b).

256 Previous dynamic rupture simulations show that fault zone wave reflections can induce  
 257 pulse-like ruptures (Harris & Day, 1997; Huang & Ampuero, 2011; Huang et al., 2014). We  
 258 observe the imprint of these wave reflections in the spatiotemporal slip rate evolution of  
 259 fault damage zone simulations (Fig. 5). These Slip pulses become a dominant feature dur-  
 260 ing earthquake rupture as the waves are reflected from the damage zone boundaries in our  
 261 earthquake cycle simulations. Similar pulse-like ruptures are also observed in homogeneous  
 262 earthquake cycle simulations for specific sets of heterogeneous friction parameters and fault  
 263 asperity dimensions (Michel et al., 2017; Barbot, 2019). Our results suggest that stress het-  
 264 erogeneities generated by slip pulses due to seismic wave reflections are primarily responsible  
 265 for the complexities in accumulated slip and variation in hypocenter distributions.

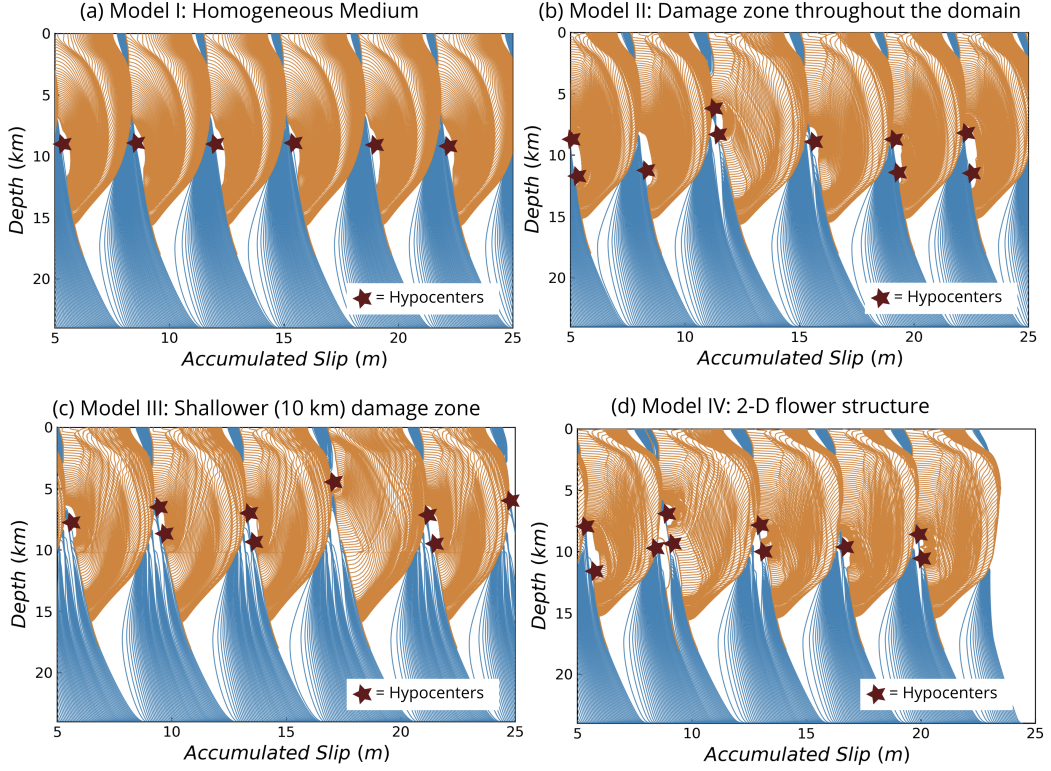


**Figure 4.** Cumulative slip contours with hypocenters shown as red stars. Multiple hypocenters close to each other represent smaller ( $M_w \sim 3$ ) and larger ( $M_w \sim 7$ ) earthquakes. The orange lines are plotted every 0.1 s during an earthquake and the blue lines are plotted every 2 yr during the interseismic period. Four different models include (a) homogeneous medium, (b) fault damage zone extending throughout the domain, (c) fault damage zone truncated at a shallower depth of 10 km, and (d) 2D flower structure. The half-width of the damage zone is 150 m in (b) and (c) and the shear wave velocity reduction is 40% of host rock. The inner damage zone in (d) is 150 m wide with 40% shear wave velocity reduction and the outer damage zone is 1.5 km wide with 20% shear wave velocity reduction.

266 We compute the moment magnitudes of simulated earthquakes to investigate the relation  
 267 between the magnitudes and cumulative number of earthquakes. The start and end of  
 268 a rupture is defined based on a threshold slip velocity of  $0.001 \text{ m s}^{-1}$ . The seismic moment  
 269 is calculated as the product of the elastic shear modulus ( $\mu$ ), the coseismic slip ( $D$ ) inte-  
 270 grated along the depth, and the rupture area. The rupture length ( $L$ ) is defined as the part  
 271 of the fault where slip is greater than 1% of the maximum coseismic slip during a certain  
 272 earthquake. Since our simulation is two-dimensional, we assume the rupture width ( $W$ ) is  
 273 the same as the rupture length. The seismic moment ( $M_o$ ) is defined as:

$$274 \quad M_o = \mu(L.W)D = \int dL \int \mu dL.D(L) \quad (6)$$

275 The moment magnitude is computed using Kanamori's (1975) scaling relation:  $M_w =$   
 276  $2/3 \log M_o - 10.7$ , where  $M_o$  is the seismic moment.

277 In our simulations, the model with homogeneous medium hosts one large earthquake  
 278 every  $\sim 100$  years. The recurrence intervals and magnitude of the earthquakes are also  
 279 fairly uniform throughout the seismic cycle. In the presence of the fault damage zone,

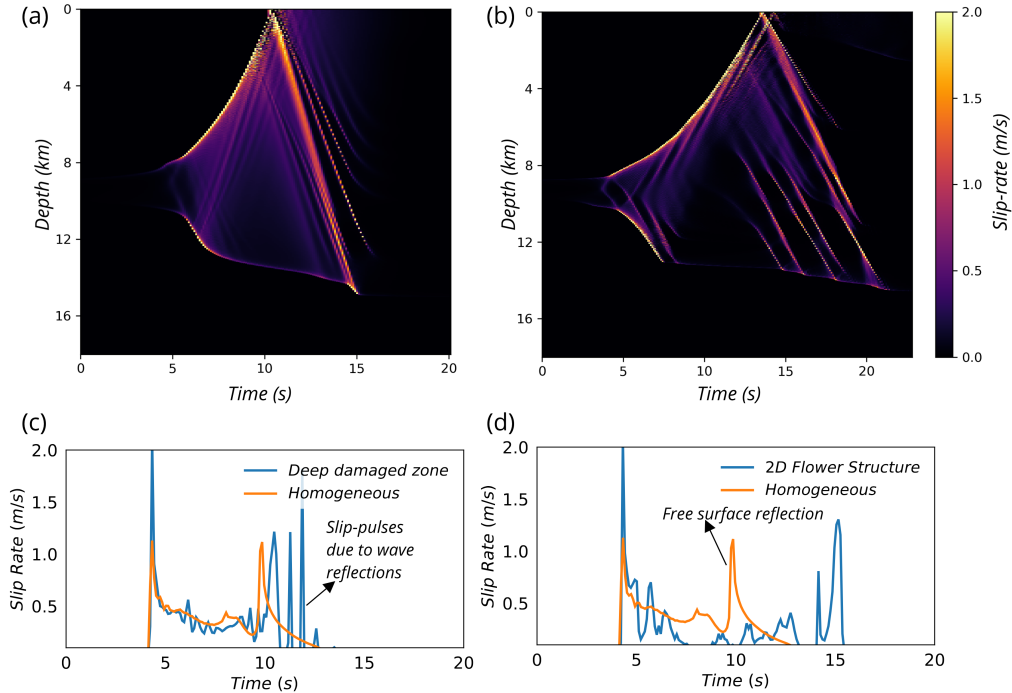


**Figure 5.** Spatiotemporal slip rate evolution demonstrating dynamic wave reflections for (a) fault damage zone extending throughout the domain, and (b) trapezoid shaped nested fault damage zone. (c) and (d) show the slip rate at a depth of 7km for (a) and (b) respectively as compared to a homogeneous medium. The ruptures begin as crack but transition to pulses due to the wave reflections.

280 we observe more complex slip history with varying earthquake magnitudes and hypocen-  
 281 ter locations. To further understand the simulated earthquake catalog, we investigate the  
 282 number of earthquakes for each magnitude range (i.e., magnitude-frequency distribution).  
 283 We combine the magnitudes for all the fault zone simulations in order to emulate a natu-  
 284 ral setting where there are multiple faults with varying fault damage zone properties and  
 285 show their cumulative magnitude frequency distribution in Fig. 6a. We observe a decrease  
 286 in the number of earthquakes as the magnitude increases from 3 to 4.5, after which the  
 287 number of earthquakes stagnates for intermediate magnitudes of 4.5 to 6. Finally we see  
 288 a sharp decrease in the number of earthquakes for the largest earthquakes. This combined  
 289 magnitude-frequency distribution is different from the Gutenberg-Richter distribution.

290 To understand the gap in the intermediate magnitude earthquakes, we examine the  
 291 envelope of the coseismic slip distributions representing the rupture area for all the simulated  
 292 earthquakes (Fig. 6b). The rupture areas of smaller earthquakes are confined within the  
 293 depth range of 3 km to 11 km (Fig. 6b). The rupture area and final slip for these subsurface  
 294 events are  $\sim 10$  times smaller than those of the surface-rupturing events. Therefore there  
 295 is two orders of gap in the moment magnitudes between the small and large events. Since  
 296 the effective normal stress and hence the fault strength is low at depths shallower than  
 297 3 km, it is harder to stop dynamic ruptures once they reach this shallow depth. When  
 298 the rupture breaks through the free surface, the magnitude of the earthquakes tend to be  
 299 much larger, which may explain the lack of intermediate magnitude earthquakes. Another  
 300 potential reason is that there is no along-strike rupture termination in our 2D models.  
 301 Generating a Gutenberg-Richter type earthquake catalogue may require multiple faults

302 with varying spatial dimensions, additional frictional or material heterogeneities, and/or  
 303 along-strike termination of spontaneous ruptures.

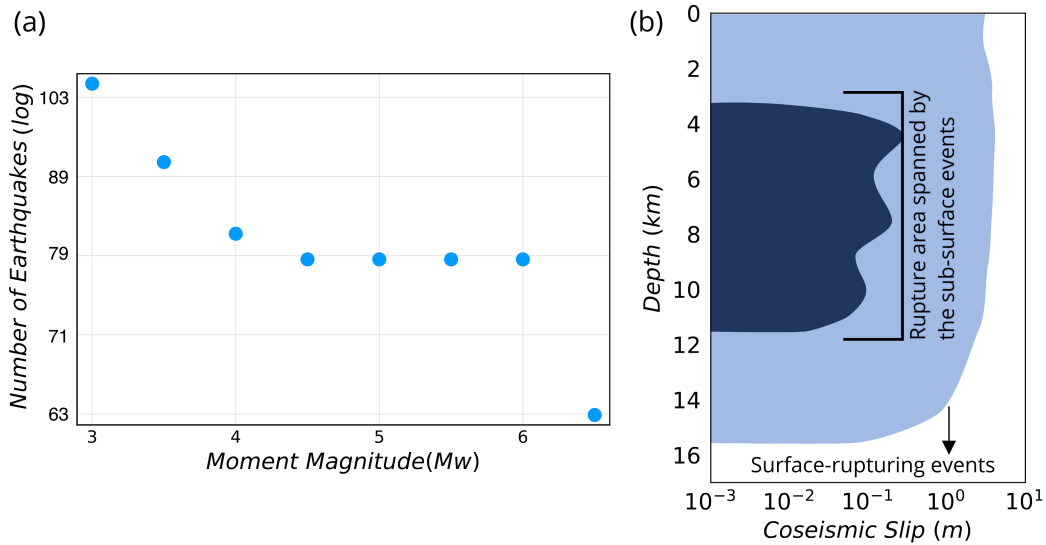


**Figure 6.** (a) Cumulative magnitude-frequency distribution for the combined simulations with multiple fault damage zone widths, depths, and rigidity contrasts. (b) The envelope of coseismic slip for the larger and smaller earthquakes against are plotted against the fault depth. We show the cumulative rupture length (and therefore rupture area) for all the larger and smaller earthquakes combined as the shaded region.

#### 4.1 Variability in Earthquake Hypocenters

304

305 Earthquakes on crustal strike-slip faults tend to occur within the top 15 km to 20 km of  
 306 the crust, known as the seismogenic zone. However, these earthquakes are not uniform along  
 307 depth, and are more correlated with the shallow crustal structure (Marone & Scholz, 1988).  
 308 Mai et al. (2005) have performed Kolmogorov-Smirnov tests on a database of finite-source  
 309 inversions and showed that the uniformity of hypocenters along depth can be statistically  
 310 rejected, especially for strike-slip faults. Other studies (Marone & Scholz, 1988; Hauksson  
 311 & Meier, 2019) have shown that the depth distribution of earthquake hypocenters may  
 312 be more bimodal, with strong clustering of earthquakes at shallow ( $\sim 5$  km) and deeper  
 313 ( $\sim 15$  km) depths. Such a bimodal distribution has also been observed in thrust fault settings  
 314 (Dal Zilio, 2020). Shallow seismicity is usually interpreted as short-term strain transients or  
 315 changes in the frictional and rheological properties of rocks along depth. The abrupt decrease  
 316 in deeper seismicity ( $\leq 15$  km) is attributed to the thermo-mechanical behavior of rocks at  
 317 these depths. We provide an alternate explanation for the bimodal distribution of seismicity  
 318 along strike-slip faults based on the geometrical extent of fault damage zones, wherein the  
 319 structural boundary of the fault damage zone produces additional stress concentration that  
 320 promotes earthquake nucleation near the boundary. Our results also suggest that frictional  
 321 and rheological effects may be a dominant mechanism for hypocenter variability when the  
 322 damaged structure is shallower than 8 km.

323 The depth distributions of earthquake hypocenters for various fault zone depths, widths  
 324 and velocity contrasts are shown in Fig. 7. In contrast to the homogeneous medium, the

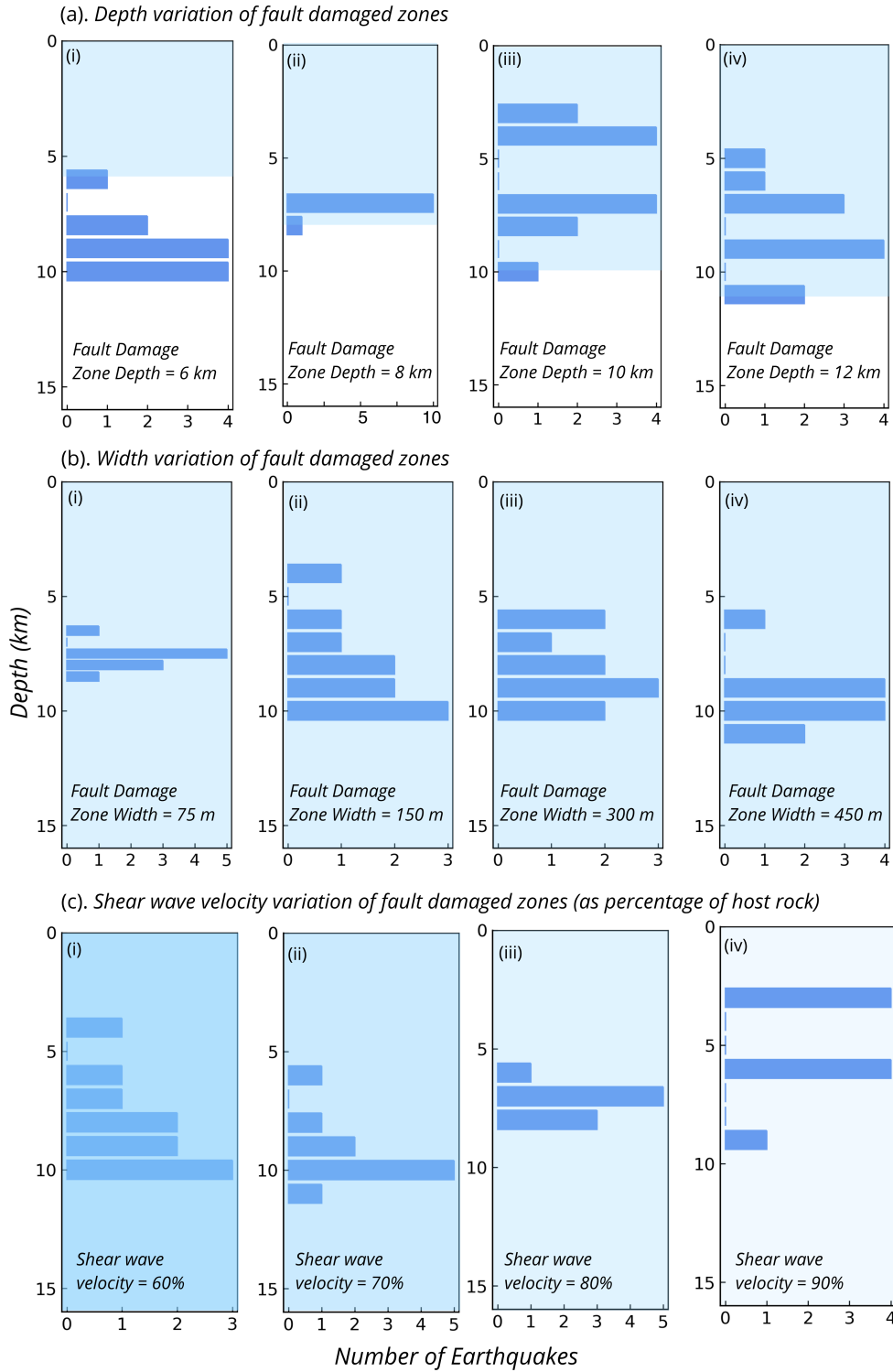


**Figure 7.** Earthquake hypocenter distribution for simulations with varying (a) fault damage zone depths, (b) widths, and (c) shear wave velocity contrasts. The shaded region shows the depth extent of damage zone and the intensity of shading shows the shear wave velocity contrast.

325 hypocenter locations vary considerably for the fault zone simulations, and the depth extent of  
 326 the fault damage zone has a pronounced effect on the hypocenter location. As demonstrated  
 327 by Fig. 7a, the maximum variability in hypocenter locations is observed when the fault  
 328 damage zone extends to the earthquake nucleation sites. As the fault zone becomes deeper,  
 329 we see a systematic downward shift in the average hypocenter location, which saturates  
 330 for a very deep fault zone extending throughout the seismogenic zone. We attribute this  
 331 variability to the sharp material discontinuity between the fault damage zone and the host  
 332 rock where shear stress changes tend to be concentrated (Bonafede et al., 2002; Rybicki &  
 333 Yamashita, 2002), resulting a number of earthquakes nucleating near this interface. For the  
 334 same depth below the shallower fault zone, the deeper fault zone leads to a smaller nucleation  
 335 size due to the reduction in elastic shear modulus, thus allowing earthquakes to nucleate at  
 336 a deeper location as the fault is loaded from below. However, when the damage zone is very  
 337 shallow, in the order of  $\sim 6$  km depth (Fig. 7a), most of the earthquakes nucleate below the  
 338 damage zone. This suggests that the interplay between the earthquake nucleation site and  
 339 damage zone boundary is an important factor influencing earthquake hypocenter locations.  
 340 Despite additional stress concentration at the fault damage zone boundary, fault loading  
 341 conditions and frictional boundary have a dominant effect on earthquake hypocenters for  
 342 very shallow fault zone. But as the fault damage zone penetrates to the nucleation site, the  
 343 fault zone effects become more critical in determining the depth distribution of seismicity.  
 344 In other words, the seismicity distribution is influenced by both the material and frictional  
 345 boundaries.

346 In fault damage zones extending throughout seismogenic depths, the increase of damage  
 347 zone width also leads to an increase in the average hypocenter depths (Fig. 7b). This is  
 348 consistent with the idea that the nucleation size is reduced as the width increases, which  
 349 should lead to a downward shift in earthquake hypocenters when the fault loaded from  
 350 below. The hypocenter locations also tend to be deeper for a higher shear wave velocity  
 351 contrast, again due to a smaller nucleation size (Fig. 7c).

352 Our simulations highlight the variable depth distribution of earthquake hypocenters  
 353 on strike-slip faults. In certain cases, a shallow fault damage zone exhibits more bimodal  
 354 distribution of hypocenters (Fig. 7a), whereas deeper fault damage zones tend to exhibit  
 355 more unimodal distribution (Fig. 7b). We also see a bimodal distribution when the shear  
 356 wave velocity contrast is very low (Fig. 7c), which can be attributed to frictional stress  
 357 concentrations. We show the hypocenter distributions from two representative simulations  
 358 of a shallow and a deep fault damage zone against various observations (Fig. 8a), wherein  
 359 the shallower damage zone shows a more bimodal distribution as compared to a deeper  
 360 damage zone (Fig. 8b). It is pertinent to note that most of the observations of seismicity  
 361 depth distribution is limited to small earthquakes, because we do not have enough record  
 362 of large earthquakes along single faults. Nevertheless, we are qualitatively able to compare  
 363 the simulated earthquake hypocenter locations with the observed hypocenter locations.

#### 364 4.2 Evolution of Peak Slip Rate and Fault Shear Stresses

365 We show the peak slip rate evolution for our simulations in Fig. 9. A homogeneous  
 366 simulation shows large recurring earthquakes, whereas smaller events emerge in a damaged  
 367 medium, caused by the interplay between the fault damage zone boundary and the nucle-  
 368 ation along the fault. In addition, we observe multiple ‘slow events’ in the presence of the  
 369 fault damage zone that do not grow to fully dynamic earthquakes. The complexities in the  
 370 number of these ‘slow events’ are elevated for a shallow fault damage zone extending to  
 371 the nucleation site (Fig. 9c). The flower structure shows a more complex peak slip rate  
 372 function (Fig. 9d) despite having fewer slow events because the inner damage zone extends  
 373 deep within the seismogenic zone. These slow events in our models occur at  $\sim 10$  km depth  
 374 (Fig. 4 b,d), close to the nucleation site and also close to the damage boundary in the  
 375 case of shallower fault damage zone (Fig. 4c). They can be interpreted as accelerations in  
 376 the slip rate that cannot grow to fully dynamic earthquakes because the stresses are not

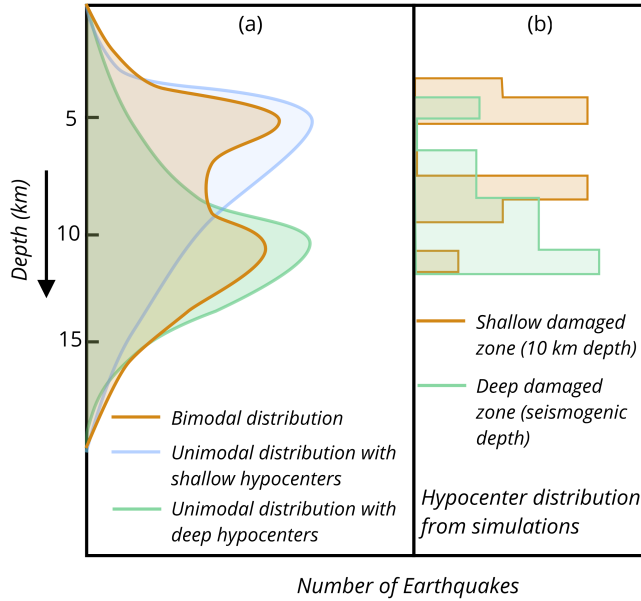


**Figure 8.** (a). Observed seismicity distribution along strike-slip faults. We show bimodal distribution (Marone & Scholz, 1988; Mai et al., 2005; Hauksson & Meier, 2019), unimodal distribution with shallow hypocenters (Powers & Jordan, 2010; Kim et al., 2016), and unimodal distribution with deep hypocenters (Hauksson & Meier, 2019). (b) Simulated hypocenter distribution for a shallow and a deep damage zone.

377 large enough to reach the dynamic regime, i.e., a failed nucleation. Slow slip events with  
 378 back-propagating pulses have previously been observed in low-velocity fault zone simulations  
 379 under the quasidynamic approximation Idini and Ampuero (2020)(EarthArXiv preprint).  
 380 These events are modeled using additional frictional strengthening. We observe a combi-  
 381 nation of slow events and dynamic ruptures in the velocity weakening regime. Our results  
 382 imply that the geometry of the damaged medium can cause additional source complexities  
 383 that are similar to seismic observations. We infer that a mature fault zone is more likely to  
 384 exhibit slow events compared to immature fault zones in strike-slip tectonic settings.

385 In order to understand the mechanism underlying the variability of earthquake hypocen-  
 386 ter locations and the scale of stress heterogeneities, we show the temporal evolution of fault  
 387 shear stresses for different types of fault zones. Fig. 10 shows the shear stress evolution  
 388 for the largest earthquake in homogeneous medium ( $L = 8$  mm), a deeper fault damage  
 389 zone, a shallow fault damage zone, and the 2D flower structure, respectively. Ruptures in  
 390 the fault zone undergo a transition from cracks to pulses predominantly after the waves are  
 391 reflected from the fault damage zone boundaries (Fig. 5a), while the homogeneous simu-  
 392 lations maintain crack-like ruptures. In addition to the observed reduction in nucleation  
 393 sizes, shear stress heterogeneities emerge during the nucleation phase in the damage zone  
 394 simulations (Fig. 10b), whereas they are absent in homogeneous medium (Fig. 10a). The  
 395 interference of multiple stress peaks very close to the nucleation site are responsible for the  
 396 variability in earthquake hypocenter locations and sizes in the fault zone simulations. The  
 397 emergence of smaller earthquakes ( $M_w \sim 3.0$ ) and the slow events are prominent when a  
 398 fault damage zone extends to the nucleation site of the earthquakes. Although earthquake  
 399 rupture velocities are slower in the fault damage zone, the stress peak amplitudes are larger  
 400 than the homogeneous medium. Overall, the two key effects of the fault damage zoned in

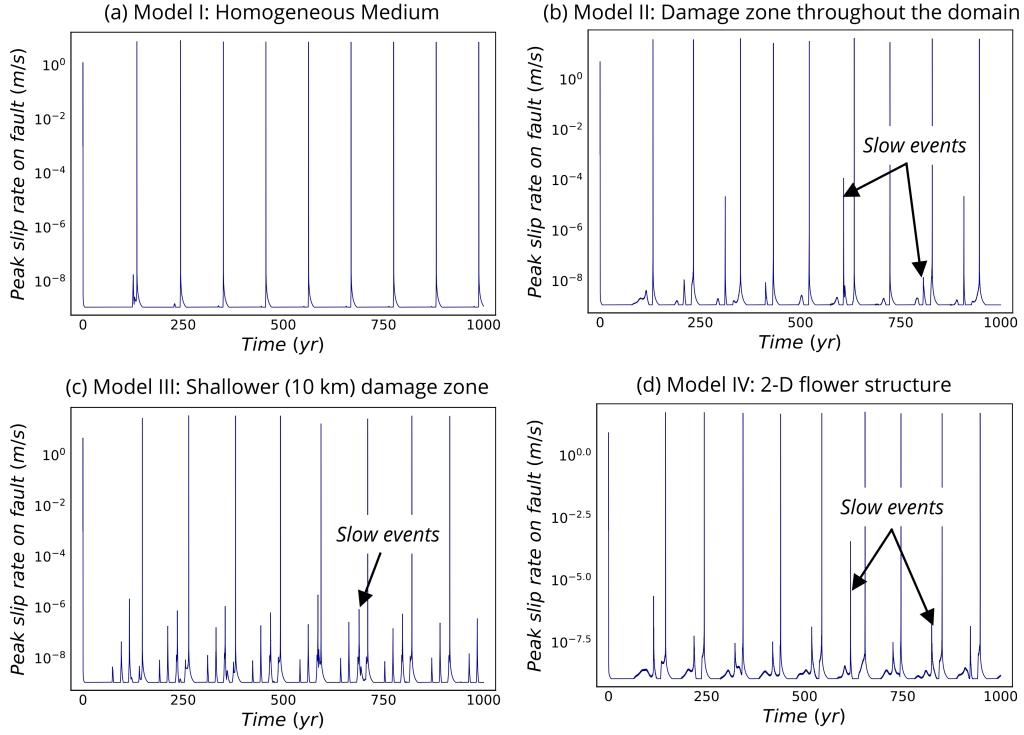


**Figure 9.** Peak slip rate function for (a) homogeneous medium, (b) deep fault damage zone, (c) shallow fault damage zone, (d) two-dimensional flower structure.

fully dynamic earthquake sequences are: (a) multiple stress peaks near the nucleation site, (b) small-scale stress heterogeneities due to dynamic wave reflections.

### 4.3 Effects of Reduced Nucleation Sizes in Homogeneous Medium

The theoretical nucleation size of a mode III rupture is directly proportional to the rigidity of the medium. Since smaller nucleation sizes also tend to give rise to complexities in earthquake cycles (Lapusta & Rice, 2003), it is imperative to isolate the effects of reduced nucleation size from the effects of dynamic wave reflections and stress heterogeneities due to the fault damage zones. In this section, we analyze a simulation where the entire medium is damaged and has a 40% shear wave velocity reduction compared to the homogeneous medium in previous simulations. The cumulative slip profile and the shear stress evolution (Fig. 11) show a clear reduction in nucleation size when compared to the undamaged homogeneous medium (Fig. 4a) as expected from theoretical predictions. Furthermore, we see a downward shift in earthquake hypocenter locations, which is also an expected phenomenon for mode III earthquake cycles due to the loading conditions (Lapusta & Rice, 2003). Another effect is the increase in recurrence intervals of the large earthquakes, which can be attributed to a reduced shear modulus in the medium (Cattania, 2019). Despite these differences, we do not observe complexities such as variations in hypocenter locations or earthquake sizes as observed in fault zone simulations. Therefore, these complexities can be attributed to dynamic wave reflections and stress heterogeneities induced by the complex nucleation phase (Fig. 10 b,c,d).

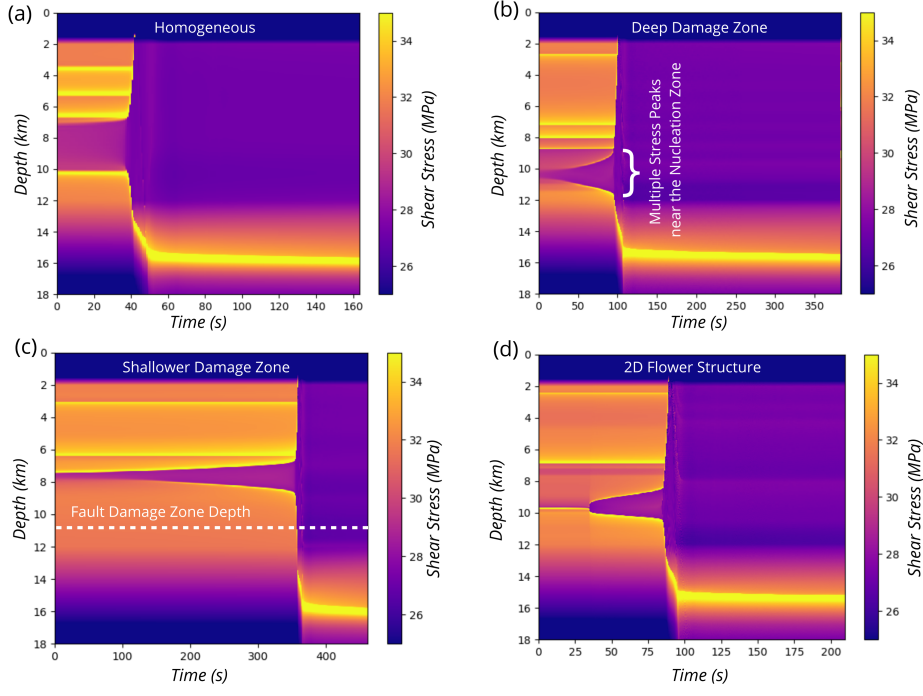


**Figure 10.** Shear stress evolution of a single earthquake including the nucleation phase shown along the fault for (a) homogeneous medium, (b) deep fault zone, (c) shallower fault zone, (d) two-dimensional flower structure.

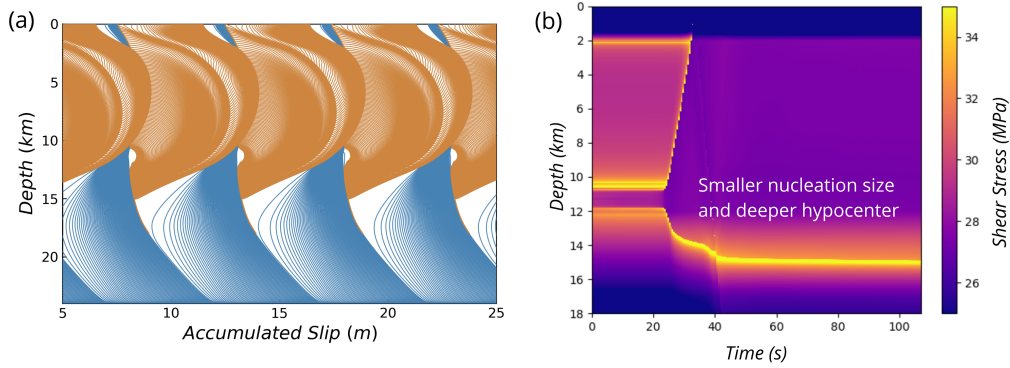


**Figure 11.** (a) Cumulative slip evolution with the orange lines plotted every 0.5s and blue lines plotted every 2yr. (b) Shear stress evolution for one earthquake when the entire medium is damaged. The shear wave velocity is 60% that of undamaged medium (compare Fig. 4a), which would effectively reduce the nucleation size by 66%. We do not see variability in hypocenter locations or earthquake magnitude.

## 5 Discussion and Conclusions

We present fully dynamic earthquake cycle models that incorporate near-fault material heterogeneities represented by a fault damage zone. We show that the fault zone waves can

421

422

423

424 lead to earthquakes with variable magnitudes and hypocenter locations. The depth distri-  
 425 bution of earthquake hypocenters is strongly affected by the fault damage zone depth, with  
 426 shallower fault zones favoring shallower hypocenters. We also see a bimodal depth distribu-  
 427 tion of earthquake hypocenters in shallow damage zones and a more unimodal distribution  
 428 in deeper damage zones. The variable nucleation locations originate from the interaction  
 429 between stress heterogeneity induced by dynamic fault zone waves and the rate and state  
 430 fault. In the shallow fault zone, the stress peaks are concentrated near the bottom of the  
 431 fault damage zone and directly correlated with the earthquake nucleation locations, whereas  
 432 the complex nucleation phase is absent in the homogeneous media.

433 Previous static and quasi-dynamic simulations have shown that perturbations in shear  
 434 and normal stress can give rise to complex seismicity (Ben-Zion, 2001; Perfettini et al., 2003).  
 435 Furthermore, observations and numerical experiments suggest that the tectonic stresses on  
 436 real faults are spatially heterogeneous (Townend & Zoback, 2000; Rivera & Kanamori,  
 437 2002), implying that the stress amplitudes are not smooth but oscillatory over space. The  
 438 emergence of persistent slip pulses after initial few seconds of rupture propagation contribute  
 439 to stress heterogeneity in our simulations. Another key observation is the emergence of  
 440 smaller, slower events in the damaged medium that do not grow to dynamic earthquakes.  
 441 These slow events are more prominent in the shallow fault zones where the depth of the fault  
 442 damage zone intersects the nucleation zone but does not extend deeper to the seismogenic  
 443 zone. This suggests that the material heterogeneities strongly influence the nucleation phase  
 444 in addition to generating dynamic reflected waves. The emergence of these slow events in  
 445 our fault damage zone simulations could potentially explain why we do not observe slow  
 446 slip events in young and immature fault zones.

447 We find that the shape and properties of damage zone can affect the stress distribution  
 448 and significantly contribute to complex seismicity even without smaller-scale frictional het-  
 449 erogeneities along fault. Earthquake magnitudes show significant variability when compared  
 450 to a homogeneous medium, but the log-linearity of the magnitude-frequency distribution is  
 451 difficult to reproduce due to the limited number of earthquakes generated in the simulations.  
 452 Observations in regional and global earthquake catalogues generally show a log-linear decay  
 453 of magnitude with increasing number of earthquakes, in agreement with the Gutenberg-  
 454 Richter distribution. However, large earthquakes along individual faults or fault sections  
 455 deviate from this behavior, showing a relatively elevated number of ‘characteristic earth-  
 456 quakes’ (Schwartz & Coppersmith, 1984; Wesnousky, 1994; Parsons et al., 2018) that follow  
 457 a gaussian distribution in addition to smaller earthquakes that follow the Gutenberg-Richter  
 458 distribution. This characteristic distribution is used as a basis for rupture forecast models,  
 459 e.g., (Field et al., 2017). We have combined the earthquakes from multiple simulations to  
 460 emulate a regional catalogue where we may have multiple faults with different fault zone  
 461 characteristics, but we ignore the interactions between these faults. In order to reproduce  
 462 a Gutenberg-Richter distribution, more complexities in the model are required. The ques-  
 463 tion still remains whether we need only material heterogeneities, or additional frictional  
 464 and stress heterogeneities in combination to emulate the Gutenberg-Richter behavior. The  
 465 current model is an idealized approximation of the material effects of fault damage zones  
 466 with small fractures. More realistic approximations would include the incorporation of vis-  
 467 coelastic and plasticity effects (Allison & Dunham, 2018; Erickson et al., 2017) and variable  
 468 pore pressure effects with depth. Furthermore, complexities in the frictional parameters  
 469 ( $a - b$ ) and  $L$  are limited to standard values that remain constant throughout simulating  
 470 time. Despite these approximations, our models provide a physical description of the effects  
 471 of material heterogeneities on the long-term behavior of strike-slip faults.

472 Our future work will be directed towards understanding the effect of fault damage  
 473 zone evolution through multiple seismic cycles. Paleoseismic studies of large strike-slip  
 474 earthquakes, limited to the past 1000-1200 years, suggest that the recurrence of large events  
 475 is non-uniform, possibly even chaotic, with large gap in seismic activity followed by multiple  
 476 seismic episodes (Grant & Sieh, 1992; Seitz et al., 1997; Fumal et al., 2002; Toké et al.,

477 2006). A time-dependent stressing history, possibly driven by the evolution of the fault  
 478 damage zone through multiple seismic episodes and aseismic creep, may better explain  
 479 the observed non-uniform recurrence intervals along mature faults. Previous experiments  
 480 and observations (Peng & Ben-Zion, 2006; Stanchits et al., 2006) have shown that the  
 481 damage can be enhanced during seismic episodes and be healed during interseismic periods.  
 482 The amount and localization of damage depends on the earthquake sizes, the interseismic  
 483 duration for which the fault is allowed to heal, and recurrence intervals of large earthquakes  
 484 (Vidale & Li, 2003; Yang, 2015). Incorporating the evolution of fault damage zone would  
 485 provide more realistic outlook on long-term structural evolution and source characteristics  
 486 of mature strike-slip faults.

## 487 Appendix A Numerical Convergence in the Simulations

488 We perform numerical convergence tests for the simulations with a narrow fault damage  
 489 zone extending throughout the model domain. The half-width of the fault damage zone is  
 490 150 m, and the shear wave velocity reduction is 40%. We use an average node-spacing of  
 491 10 m, 15 m, 20 m and 40 m. The comparison between the peak slip rate and the differential  
 492 slip for a large earthquake is shown in Fig. A1. The comparison of peak slip rate for  
 493 simulations with different node spacings demonstrates that the onset of earthquakes are the  
 494 same for the different node spacings. Furthermore, Fig. A1 b shows that the differential slip  
 495 for different node spacings are the same, implying that the earthquake size is independent  
 496 of mesh size. The shape of the differential slip shown in the inset zoom figure (Fig. A1 b)  
 497 suggests all the features are not preserved for an average node spacing of 40 m, but they are  
 498 preserved for all the other node spacings. Based on this convergence study, we have chosen  
 an average node spacing of 20 m for our study.

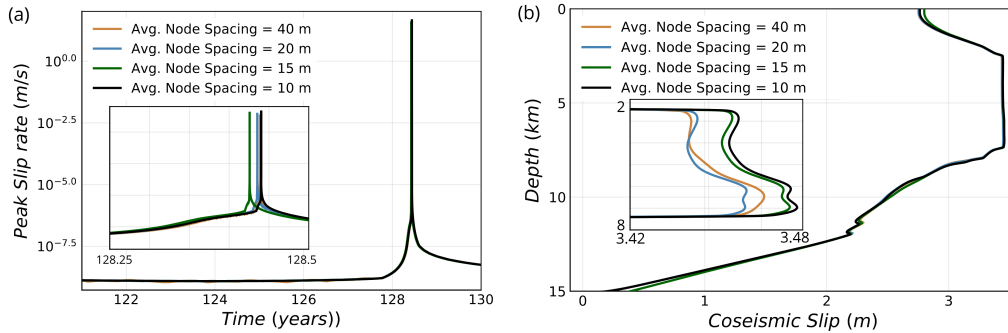


**Figure A1.** (a) Peak slip rate shown for multiple node spacings, (b) Differential slip of one earthquake shown for multiple node spacings.

499

## 500 Acknowledgments

501 This study was supported by the University of Michigan. We thank the editor — — —  
 502 and reviewers — — — for their helpful comments. P.T thanks Daning Huang for help with  
 503 the numerical procedure for implementing the Algebraic Multigrid for quasi-static solver.  
 504 The code used to perform the numerical simulations is available on github: [https://](https://github.com/thehalfspace/eqcycle)  
 505 [github.com/thehalfspace/eqcycle](https://github.com/thehalfspace/eqcycle). GMT (Wessel et al., 2013) was used to create some  
 506 figures.

## References

- Abdelmeguid, M., Ma, X., & Elbanna, A. (2019). A novel hybrid finite element-spectral boundary integral scheme for modeling earthquake cycles: Application to rate and state faults with low-velocity zones. *Journal of Geophysical Research: Solid Earth*.
- Albertini, G., & Kammer, D. S. (2017). Off-fault heterogeneities promote supershear transition of dynamic mode II cracks. *Journal of Geophysical Research: Solid Earth*, *122*(8), 6625–6641.
- Allison, K. L., & Dunham, E. M. (2018). Earthquake cycle simulations with rate-and-state friction and power-law viscoelasticity. *Tectonophysics*, *733*, 232–256.
- Barbot, S. (2019). Slow-slip, slow earthquakes, period-two cycles, full and partial ruptures, and deterministic chaos in a single asperity fault. *Tectonophysics*, *768*, 228171.
- Barbot, S., Lapusta, N., & Avouac, J.-P. (2012). Under the hood of the earthquake machine: Toward predictive modeling of the seismic cycle. *Science*, *336*(6082), 707–710. Retrieved from <http://science.sciencemag.org/content/336/6082/707> doi: 10.1126/science.1218796
- Ben-Zion, Y. (2001). Dynamic ruptures in recent models of earthquake faults. *Journal of the Mechanics and Physics of Solids*, *49*(9), 2209–2244.
- Bezanson, J., Edelman, A., Karpinski, S., & Shah, V. B. (2017). Julia: A fresh approach to numerical computing. *SIAM review*, *59*(1), 65–98.
- Blanpied, M., Lockner, D., & Byerlee, J. (1991). Fault stability inferred from granite sliding experiments at hydrothermal conditions. *Geophysical Research Letters*, *18*(4), 609–612.
- Blanpied, M. L., Lockner, D. A., & Byerlee, J. D. (1995). Frictional slip of granite at hydrothermal conditions. *Journal of Geophysical Research: Solid Earth*, *100*(B7), 13045–13064.
- Bonafede, M., Parenti, B., & Rivalta, E. (2002). On strike-slip faulting in layered media. *Geophysical Journal International*, *149*(3), 698–723.
- Caine, J. S., Evans, J. P., & Forster, C. B. (1996). Fault zone architecture and permeability structure. *Geology*, *24*(11), 1025–1028.
- Carlson, J. M., & Langer, J. (1989). Properties of earthquakes generated by fault dynamics. *Physical Review Letters*, *62*(22), 2632.
- Cattania, C. (2019). Complex earthquake sequences on simple faults. *Geophysical Research Letters*, *46*(17-18), 10384–10393.
- Chester, F., & Logan, J. M. (1986). Implications for mechanical properties of brittle faults from observations of the punchbowl fault zone, California. *Pure and applied geophysics*, *124*(1-2), 79–106.
- Chester, F. M., Evans, J. P., & Biegel, R. L. (1993). Internal structure and weakening mechanisms of the San Andreas fault. *Journal of Geophysical Research: Solid Earth*, *98*(B1), 771–786.
- Cochard, A., & Madariaga, R. (1996). Complexity of seismicity due to highly rate-dependent friction. *Journal of Geophysical Research: Solid Earth*, *101*(B11), 25321–25336.
- Dal Zilio, L. (2020). Bimodal seismicity in the Himalaya controlled by fault friction and geometry. In *Cross-scale modeling of mountain building and the seismic cycle: From alps to Himalaya* (pp. 67–93). Springer.
- Day, S. M., Dalguer, L. A., Lapusta, N., & Liu, Y. (2005). Comparison of finite difference and boundary integral solutions to three-dimensional spontaneous rupture. *Journal of Geophysical Research: Solid Earth*, *110*(B12).
- Dieterich, J. H. (1979). Modeling of rock friction: 1. experimental results and constitutive equations. *Journal of Geophysical Research: Solid Earth*, *84*(B5), 2161–2168. Retrieved from <https://agupubs.onlinelibrary.wiley.com/doi/abs/10.1029/JB084iB05p02161> doi: 10.1029/JB084iB05p02161
- Erickson, B. A., & Dunham, E. M. (2014). An efficient numerical method for earthquake cycles in heterogeneous media: Alternating subbasin and surface-rupturing events on faults crossing a sedimentary basin. *Journal of Geophysical Research: Solid Earth*, *119*(4), 3290–3316.

- 562 Erickson, B. A., Dunham, E. M., & Khosravifar, A. (2017). A finite difference method for off-  
 563 fault plasticity throughout the earthquake cycle. *Journal of the Mechanics and Physics*  
 564 *of Solids*, *109*, 50 - 77. Retrieved from [http://www.sciencedirect.com/science/](http://www.sciencedirect.com/science/article/pii/S0022509617305069)  
 565 [article/pii/S0022509617305069](http://www.sciencedirect.com/science/article/pii/S0022509617305069) doi: <https://doi.org/10.1016/j.jmps.2017.08.002>
- 566 Fialko, Y., Sandwell, D., Agnew, D., Simons, M., Shearer, P., & Minster, B. (2002). De-  
 567 formation on nearby faults induced by the 1999 hector mine earthquake. *Science*,  
 568 *297*(5588), 1858–1862.
- 569 Field, E. H., Jordan, T. H., Page, M. T., Milner, K. R., Shaw, B. E., Dawson, T. E., ...  
 570 others (2017). A synoptic view of the third uniform california earthquake rupture  
 571 forecast (ucerf3). *Seismological Research Letters*, *88*(5), 1259–1267.
- 572 Fumal, T., Weldon, R., Biasi, G., Dawson, T., Seitz, G., Frost, W., & Schwartz, D. (2002).  
 573 Evidence for large earthquakes on the san andreas fault at the wrightwood, california,  
 574 paleoseismic site: Ad 500 to present. *Bulletin of the Seismological Society of America*,  
 575 *92*(7), 2726–2760.
- 576 Grant, L., & Sieh, K. (1992). Irregular recurrence times and increased seismic hazard from  
 577 earthquakes on the carrizo segment of the san andreas fault, southern california. In  
 578 *Proc. of the 35th ann. meeting of the assoc. of engineering geologists* (pp. 2–9).
- 579 Harris, R. A., & Day, S. M. (1997). Effects of a low-velocity zone on a dynamic rupture.  
 580 *Bulletin of the Seismological Society of America*, *87*(5), 1267–1280.
- 581 Hauksson, E., & Meier, M.-A. (2019). Applying depth distribution of seismicity to de-  
 582 termine thermo-mechanical properties of the seismogenic crust in southern california:  
 583 comparing lithotectonic blocks. *Pure and Applied Geophysics*, *176*(3), 1061–1081.
- 584 Hillers, G., Ben-Zion, Y., & Mai, P. M. (2006, January). Seismicity on a fault con-  
 585 trolled by rate- and state-dependent friction with spatial variations of the critical  
 586 slip distance. *Journal of Geophysical Research (Solid Earth)*, *111*, B01403. doi:  
 587 [10.1029/2005JB003859](https://doi.org/10.1029/2005JB003859)
- 588 Huang, Y. (2018). Earthquake rupture in fault zones with along-strike material heterogene-  
 589 ity. *Journal of Geophysical Research: Solid Earth*.
- 590 Huang, Y., & Ampuero, J.-P. (2011). Pulse-like ruptures induced by low-velocity fault  
 591 zones. *Journal of Geophysical Research: Solid Earth*, *116*(B12).
- 592 Huang, Y., Ampuero, J.-P., & Helmberger, D. V. (2014). Earthquake ruptures modulated by  
 593 waves in damaged fault zones. *Journal of Geophysical Research: Solid Earth*, *119*(4),  
 594 3133–3154.
- 595 Idini, B., & Ampuero, J.-P. (2020). Fault-zone damage promotes pulse-like rupture and  
 596 rapid-tremor-reversals.
- 597 Jiang, J., & Lapusta, N. (2016, June). Deeper penetration of large earthquakes on seismically  
 598 quiescent faults. *Science*, *352*, 1293–1297. doi: [10.1126/science.aaf1496](https://doi.org/10.1126/science.aaf1496)
- 599 Kaneko, Y., Ampuero, J.-P., & Lapusta, N. (2011, October). Spectral-element simulations of  
 600 long-term fault slip: Effect of low-rigidity layers on earthquake-cycle dynamics. *Jour-  
 601 nal of Geophysical Research (Solid Earth)*, *116*, B10313. doi: [10.1029/2011JB008395](https://doi.org/10.1029/2011JB008395)
- 602 Kaneko, Y., Lapusta, N., & Ampuero, J.-P. (2008). Spectral element modeling of spon-  
 603 taneous earthquake rupture on rate and state faults: Effect of velocity-strengthening  
 604 friction at shallow depths. *Journal of Geophysical Research: Solid Earth*, *113*(B9).
- 605 Kim, W., Hong, T.-K., Lee, J., & Taira, T. (2016). Seismicity and fault geometry of the  
 606 san andreas fault around parkfield, california and their implications. *Tectonophysics*,  
 607 *677*, 34–44.
- 608 Lapusta, N., & Rice, J. R. (2003). Nucleation and early seismic propagation of small and  
 609 large events in a crustal earthquake model. *Journal of Geophysical Research: Solid*  
 610 *Earth*, *108*(B4).
- 611 Lapusta, N., Rice, J. R., Ben-Zion, Y., & Zheng, G. (2000). Elastodynamic analysis  
 612 for slow tectonic loading with spontaneous rupture episodes on faults with rate- and  
 613 state-dependent friction. *Journal of Geophysical Research: Solid Earth*, *105*(B10),  
 614 23765–23789. Retrieved from [https://agupubs.onlinelibrary.wiley.com/doi/](https://agupubs.onlinelibrary.wiley.com/doi/abs/10.1029/2000JB900250)  
 615 [abs/10.1029/2000JB900250](https://agupubs.onlinelibrary.wiley.com/doi/abs/10.1029/2000JB900250) doi: [10.1029/2000JB900250](https://doi.org/10.1029/2000JB900250)
- 616 Lewis, M. A., & Ben-Zion, Y. (2010). Diversity of fault zone damage and trapping structures

- 617 in the parkfield section of the san andreas fault from comprehensive analysis of near  
618 fault seismograms. *Geophysical Journal International*, 183(3), 1579–1595.
- 619 Li, Y.-G., & Leary, P. (1990). Fault zone trapped seismic waves. *Bulletin of the Seismological*  
620 *Society of America*, 80(5), 1245–1271.
- 621 Li, Y.-G., & Vernon, F. L. (2001). Characterization of the san jacinto fault zone near anza,  
622 california, by fault zone trapped waves. *Journal of Geophysical Research: Solid Earth*,  
623 106(B12), 30671–30688.
- 624 Lockner, D. A., Morrow, C., Moore, D., & Hickman, S. (2011). Low strength of deep san  
625 andreas fault gouge from safod core. *Nature*, 472(7341), 82.
- 626 Ma, X., & Elbanna, A. (2015). Effect of off-fault low-velocity elastic inclusions on supershear  
627 rupture dynamics. *Geophysical Journal International*, 203(1), 664–677.
- 628 Mai, P. M., Spudich, P., & Boatwright, J. (2005). Hypocenter locations in finite-source  
629 rupture models. *Bulletin of the Seismological Society of America*, 95(3), 965–980.
- 630 Marone, C., & Scholz, C. (1988). The depth of seismic faulting and the upper transition  
631 from stable to unstable slip regimes. *Geophysical Research Letters*, 15(6), 621–624.
- 632 Michel, S., Avouac, J.-P., Lapusta, N., & Jiang, J. (2017). Pulse-like partial ruptures and  
633 high-frequency radiation at creeping-locked transition during megathrust earthquakes.  
634 *Geophysical Research Letters*, 44(16), 8345–8351.
- 635 Mogi, K. (1962). Magnitude-frequency relation for elastic shocks accompanying fractures of  
636 various materials and some related problems in earthquakes. *Bull. Earthq. Res. Inst.*,  
637 40, 831–853.
- 638 Parsons, T., Geist, E. L., Console, R., & Carluccio, R. (2018). Characteristic earthquake  
639 magnitude frequency distributions on faults calculated from consensus data in californi-  
640 a. *Journal of Geophysical Research: Solid Earth*, 123(12), 10–761.
- 641 Pelties, C., Huang, Y., & Ampuero, J.-P. (2015). Pulse-like rupture induced by three-  
642 dimensional fault zone flower structures. *Pure and Applied Geophysics*, 172(5), 1229–  
643 1241.
- 644 Peng, Z., & Ben-Zion, Y. (2006, Mar 01). Temporal changes of shallow seismic velocity  
645 around the karadere-düzce branch of the north anatolian fault and strong ground  
646 motion. *pure and applied geophysics*, 163(2), 567–600. Retrieved from <https://doi.org/10.1007/s00024-005-0034-6> doi: 10.1007/s00024-005-0034-6
- 647  
648 Perfettini, H., Schmittbuhl, J., & Cochard, A. (2003). Shear and normal load perturbations  
649 on a two-dimensional continuous fault: 2. dynamic triggering. *Journal of Geophysical*  
650 *Research: Solid Earth*, 108(B9).
- 651 Perrin, C., Manighetti, I., Ampuero, J.-P., Cappa, F., & Gaudemer, Y. (2016). Location  
652 of largest earthquake slip and fast rupture controlled by along-strike change in fault  
653 structural maturity due to fault growth. *Journal of Geophysical Research: Solid Earth*,  
654 121(5), 3666–3685. Retrieved from <https://agupubs.onlinelibrary.wiley.com/doi/abs/10.1002/2015JB012671> doi: 10.1002/2015JB012671
- 655  
656 Powers, P. M., & Jordan, T. H. (2010). Distribution of seismicity across strike-slip faults  
657 in california. *Journal of Geophysical Research: Solid Earth*, 115(B5).
- 658 Rice, J. R. (1993). Spatio-temporal complexity of slip on a fault. *Journal of Geophysical*  
659 *Research: Solid Earth*, 98(B6), 9885–9907.
- 660 Rice, J. R., & Ben-Zion, Y. (1996). Slip complexity in earthquake fault models. *Proceedings*  
661 *of the National Academy of Sciences*, 93(9), 3811–3818.
- 662 Rivera, L., & Kanamori, H. (2002). Spatial heterogeneity of tectonic stress and friction in  
663 the crust. *Geophysical Research Letters*, 29(6), 12–1.
- 664 Rubin, A., & Ampuero, J.-P. (2005). Earthquake nucleation on (aging) rate and state faults.  
665 *Journal of Geophysical Research: Solid Earth*, 110(B11).
- 666 Ruge, J. W., & Stüben, K. (1987). Algebraic multigrid. In *Multigrid methods* (pp. 73–130).  
667 SIAM.
- 668 Ruina, A. (1983). Slip instability and state variable friction laws. *Journal of Geophysi-*  
669 *cal Research: Solid Earth*, 88(B12), 10359–10370. Retrieved from <https://agupubs.onlinelibrary.wiley.com/doi/abs/10.1029/JB088iB12p10359> doi: 10.1029/JB088iB12p10359
- 670  
671

- 672 Rundle, J. B. (1989). A physical model for earthquakes: 3. thermodynamical approach and  
 673 its relation to nonclassical theories of nucleation. *Journal of Geophysical Research:*  
 674 *Solid Earth*, *94*(B3), 2839-2855. Retrieved from <https://agupubs.onlinelibrary>  
 675 [.wiley.com/doi/abs/10.1029/JB094iB03p02839](https://agupubs.onlinelibrary.wiley.com/doi/abs/10.1029/JB094iB03p02839) doi: 10.1029/JB094iB03p02839
- 676 Rundle, J. B., & Jackson, D. D. (1977). Numerical simulation of earthquake sequences.  
 677 *Bulletin of the Seismological Society of America*, *67*(5), 1363–1377.
- 678 Rybicki, K., & Yamashita, T. (2002). On faulting in inhomogeneous media. *Geophysical*  
 679 *research letters*, *29*(10).
- 680 Scholz, C. (1968). The frequency-magnitude relation of microfracturing in rock and its  
 681 relation to earthquakes. *Bulletin of the seismological society of America*, *58*(1), 399–  
 682 415.
- 683 Scholz, C. H. (1998). Earthquakes and friction laws. *Nature*, *391*(6662), 37.
- 684 Schwartz, D. P., & Coppersmith, K. J. (1984). Fault behavior and characteristic earth-  
 685 quakes: Examples from the wasatch and san andreas fault zones. *Journal of Geophys-*  
 686 *ical Research: Solid Earth*, *89*(B7), 5681-5698. Retrieved from <https://agupubs>  
 687 [.onlinelibrary.wiley.com/doi/abs/10.1029/JB089iB07p05681](https://agupubs.onlinelibrary.wiley.com/doi/abs/10.1029/JB089iB07p05681) doi: 10.1029/  
 688 JB089iB07p05681
- 689 Seitz, G., Weldon II, R., & Biasi, G. P. (1997). The pitman canyon paleoseismic record:  
 690 A re-evaluation of southern san andreas fault segmentation. *Journal of Geodynamics*,  
 691 *24*(1-4), 129–138.
- 692 Shaw, B. E. (1995). Frictional weakening and slip complexity in earthquake faults. *Journal*  
 693 *of Geophysical Research: Solid Earth*, *100*(B9), 18239–18251.
- 694 Sibson, R. (1977). Fault rocks and fault mechanisms. *Journal of the Geological Society*,  
 695 *133*(3), 191–213.
- 696 Stanchits, S., Vinciguerra, S., & Dresen, G. (2006, Jun 01). Ultrasonic velocities, acoustic  
 697 emission characteristics and crack damage of basalt and granite. *pure and applied*  
 698 *geophysics*, *163*(5), 975–994. Retrieved from <https://doi.org/10.1007/s00024-006>  
 699 [-0059-5](https://doi.org/10.1007/s00024-006-0059-5) doi: 10.1007/s00024-006-0059-5
- 700 Thurber, C., Roecker, S., Roberts, K., Gold, M., Powell, L., & Rittger, K. (2003). Earth-  
 701 quake locations and three-dimensional fault zone structure along the creeping section  
 702 of the san andreas fault near parkfield, ca: Preparing for safod. *Geophysical Research*  
 703 *Letters*, *30*(3).
- 704 Toké, N. A., Arrowsmith, J. R., Young, J. J., & Crosby, C. J. (2006). Paleoseismic and  
 705 postseismic observations of surface slip along the parkfield segment of the san andreas  
 706 fault. *Bulletin of the Seismological Society of America*, *96*(4B), S221–S238.
- 707 Townend, J., & Zoback, M. D. (2000). How faulting keeps the crust strong. *Geology*, *28*(5),  
 708 399–402.
- 709 Unsworth, M. J., Malin, P. E., Egbert, G. D., & Booker, J. R. (1997). Internal structure of  
 710 the san andreas fault at parkfield, california. *Geology*, *25*(4), 359–362.
- 711 Vidale, J. E., & Li, Y.-G. (2003). Damage to the shallow landers fault from the nearby  
 712 hector mine earthquake. *Nature*, *421*(6922), 524–526.
- 713 Weng, H., Yang, H., Zhang, Z., & Chen, X. (2016). Earthquake rupture extents and  
 714 coseismic slips promoted by damaged fault zones. *Journal of Geophysical Research:*  
 715 *Solid Earth*, *121*(6), 4446–4457.
- 716 Wesnousky, S. G. (1994). The gutenbergrichter or characteristic earthquake distribution,  
 717 which is it? *Bulletin of the Seismological Society of America*, *84*(6), 1940. Retrieved  
 718 from <http://dx.doi.org/>
- 719 Wessel, P., Smith, W. H., Scharroo, R., Luis, J., & Wobbe, F. (2013). Generic mapping  
 720 tools: improved version released. *Eos, Transactions American Geophysical Union*,  
 721 *94*(45), 409–410.
- 722 Wu, J., Holé, J. A., & Snoke, J. A. (2010). Fault zone structure at depth from differential  
 723 dispersion of seismic guided waves: evidence for a deep waveguide on the san andreas  
 724 fault. *Geophysical Journal International*, *182*(1), 343–354.
- 725 Yang, H. (2015). Recent advances in imaging crustal fault zones: A review. *Earthquake*  
 726 *Science*, *28*(2), 151–162.